HHS Public Access

Author manuscript

Biotechnol Bioeng. Author manuscript; available in PMC 2021 March 01.

Published in final edited form as:

Biotechnol Bioeng. 2020 March ; 117(3): 879–885. doi:10.1002/bit.27240.

Development of Isoporous Microslit Silicon Nitride Membranes for Sterile Filtration Applications

Evan Wright[1,§], **Joshua J. Miller**[2,§], **Matthew Csordas**[1], **Andrew R. Gosselin**[2], **Jared A. Carter**[2], **James L. McGrath**[3], **David R. Latulippe**[*,1], **James A. Roussie**[*,2]

[1]McMaster University, Department of Chemical Engineering, Hamilton, Ontario CANADA

[2]SiMPore Inc., 150 Lucius Gordon Drive, Suite 110, West Henrietta, New York USA

[3]University of Rochester, Department of Biomedical Engineering, Rochester, New York USA

Abstract

The widely used 0.2/0.22 μm polymer sterile filters were developed for small molecule and protein sterile filtration and are not well-suited for the production of large non-protein biological therapeutics, resulting in significant yield loss and production cost increases. Here, we report on the first-ever development of membranes with isoporous sub-0.2 μm rectangular prism pores using silicon micromachining to produce microslit silicon nitride (MSN) membranes. The very high porosity (~33%) and ultrathin nature of the 0.2 μm MSN membranes is a dramatically different structure than traditional 0.2/0.22 μm polymer sterile filter, which yielded comparable performance properties (including gas and hydraulic permeance, maximum differential pressure tolerance, nanoparticle sieving/fouling behavior). The results from bacteria retention tests, conducted according to the guidance of regulatory agencies, demonstrated that the 0.2 μm MSN membranes can be effectively used as sterile filters. It is believed that the results and technologies presented in this work will find future utility in the production of non-protein biological therapeutics and in other biological and biomedical applications.

Keywords

Biological Therapeutics; Sterile Filtration; Silicon Nanomembranes

Current Good Manufacturing Practice (cGMP) standards for the production of biological therapeutics rely on sterile filtration processes using microporous polymeric membranes to remove any potential bioburden in order to ensure the safety of the final formulation. Absent of aseptic production methods, the U.S. Food and Drug Administration (FDA) demands the incorporation of a final sterile filtration step to remove any potential microbial contaminants. The definition of a sterile filter is based on the retention of *Brevundimonas diminuta* (*B. diminuta*), a bacterium whose size is often reported in the range of 0.4 μm (Wang et al. 2008) to 0.8 μm under fully hydrated conditions (Harp et al. 2015). Specifically, a membrane

[*]Corresponding Authors: James Roussie, SiMPore Inc., 150 Lucius Gordon Drive, Suite 110, West Henrietta, New York, 14586, USA. Phone: +1 (585) 214-0585. jroussie@simpore.com; David Latulippe, Dept. of Chemical Engineering, McMaster University, 1280 Main St. West, Hamilton, Ontario, L8S 4L7, Canada. Phone: +1 (905) 525-9140 × 24011. latulippe@mcmaster.ca.
[§]Co-first authors

will achieve a 0.2 μm sterile filter designation according to the complete removal of *B. diminuta* when challenged with 10^7 *B. diminuta* per cm^2 of membrane surface area (FDA 2004). It is worth noting that this 0.2 μm designation is not strictly based on the pore size properties, but is known to depend on several interacting factors including the formulation conditions and operating pressure (Meltzer & Jornitz 2003).

The use of sterile filtration membranes in the production of proteinaceous biological therapeutics is not a significant technical challenge due to the much smaller size of the therapeutic product relative to the typical membrane's pore size rating. However, recent advances in the development of larger (i.e., > 50 nm average diameter) bio-pharmaceutical products, such as extracellular vesicles, antibody-conjugated drug particles, and viruses, have created a significant challenge in downstream processing operations. For instance, it has been shown that the yield loss during sterile filtration of a therapeutic rhabdovirus was greater than 75% for four polymeric membranes from three different suppliers (Shoaebargh et al. 2018); similar issues have been observed in the purification of other therapeutic viruses (Bandeira et al. 2012) and traditional viral vaccine products (Kon et al. 2016). Also, it has also been reported that the yield loss of engineered extracellular vesicles for immunotherapy reached as high as 80% when using a conventional 0.22 μm pore size polymeric membrane (Lamparski et al. 2002). An alternative strategy is use aseptic processing (Ausubel et al. 2012), which is undesirable due to the added complexity and cost. Thus, there is a need for new membrane filtration technologies that are more suitable for the downstream processing of large-sized biological therapeutics.

Micromachined membranes with slit-shaped (i.e., rectangular prism) pores are promising candidates since the width of their slit openings can be defined to specify the desired sieving behavior, while the length of their slit openings can be defined to specify their overall permeance and fouling properties. Previous lab-scale studies were performed on membranes with slit widths greater than 1 μm (Bromley et al. 2002; Chandler & Zydney 2006; Warkiani et al. 2015) or less than 30 nm (Fissell et al. 2009; Kanani et al. 2010). To the best of our knowledge, no studies to date have developed nor tested a membrane with slit pore dimensions appropriate for sterile filtration applications. Here, we report on the first development of isoporous membranes with slit-shaped pores of targeted 0.2 μm width along with the characterization of their permeability, particle sieving and fouling, and bacteria retention. The microfabrication process we developed to create these ultrathin (200 nm thick) silicon nitride membranes with precision slit pores is shown in Figure 1 (see Materials and Methods section for more details). Each microslit silicon nitride (MSN) membrane chip (5.4×5.4 mm in size) possessed four 0.3×3 mm membrane windows for a total membrane area of 3.6 mm^2. Each membrane window contained a regular array of precisely spaced slit pores and their 1:1 spacing between their narrow width resulted in an overall membrane porosity of approximately 33% (Figure 1B). The achieved dimension of the slit width was 0.186 ± 0.012 μm (mean ± standard deviation; n = 5), with a targeted slit length of 10 μm. Processing-dependent factors resulted in an approximate 7% difference in achieved versus targeted slit dimensions (Figure 1D). Despite this difference, we refer to these membranes as 0.2 μm MSN membranes for simplicity throughout this study.

To assess the performance of the MSN membranes, we measured the liquid permeance and maximum differential pressure tolerance (often referred to as burst pressure) at different slit widths (0.2, 0.5, and 1.0 μm); we also measured gas permeance as an additional characterization of these novel membrane structures. As an additional pore size comparison, nanoporous silicon nitride (NPN) membranes with cylindrical pores of average 60 nm diameter (DesOrmeaux et al. 2014; Gillmer et al. 2017) were also tested. The 0.2 μm MSN membranes, which had the highest porosity, displayed the highest nitrogen gas permeance (Figure 2B). However, we observed the hydraulic permeance fell between that of the wider 0.5 and 1.0 μm MSN membranes (Figure 2A) due to these latter two having only one-third to one-half the porosity of 0.2 μm MSN membranes, while the NPN membrane (with the smallest pore size) displayed the lowest hydraulic permeability (Figure 2A). Moreover, the maximum differential pressure tolerance for the 0.2 μm MSN membrane was approximately 1.8-times higher than those for the other two MSN membranes that were twice as thick (Figure 2C). All else remaining constant, thinner membranes should possess proportionally lower differential pressure tolerances (Gillmer et al. 2017). However, increasing the porosity of a membrane increases its flexibility and so raises its differential pressure tolerance by providing a means for strain relief (Gillmer et al. 2017). Our data suggests that the 3-times greater porosity of the 0.2 μm MSN membranes, compared to the 0.5 μm and 1.0 μm MSN membranes, may have compensated for its 2-times lower thickness and resulted in its higher differential pressure tolerance.

Next, the filtration performance of the 0.2 μm MSN membranes was assessed using buffer solutions containing polystyrene nanoparticles. The four sizes of nanoparticles (nominal diameters of 0.06, 0.18, 0.51, and 0.84 μm) were chosen specifically to span the slit width dimension; a small amount of surfactant (0.01% v/v Tween-20) was included in the nanoparticle solution to minimize the extent of nanoparticle–nanoparticle and nanoparticle–membrane interactions (Pazouki et al. 2019). The four panels in Figure 3A display the transmembrane pressure (TMP) profiles for the constant flux filtration tests that were conducted with each size of nanoparticle. Overall, the results were remarkably consistent across the triplicate testing. The initial TMP was very low (~0.1 kPa as shown in inset of the top panel of Figure 3A), due to the high permeance of the 0.2 μm MSN membranes. For the smallest nanoparticle (0.06 μm), there was no detectable increase in TMP during the entire duration of the constant flux filtration test. For the three other nanoparticles, although there was some variation between runs, overall the measured TMP profiles were fairly linear with respect to the total amount of filtrate collected. All of the measured TMP profiles were well described using the model predictions for the formation of a spherical particle cake layer on the membrane surface (Bowen & Jenner 1995); the exact details of the model are provided in the Supplementary Online Material

Our analysis of the amount of nanoparticles in the filtrate samples (as percentage of those in the corresponding feed sample) is shown in Figure 3B. We found that the smallest 0.06 μm nanoparticles were essentially completely transmitted through both 0.2 μm MSN membranes (97 ± 2%) and conventional 0.22 μm Durapore® membranes (92 ± 5%). The results for the 0.18 μm nanoparticles are particularly interesting. For the 0.2 μm MSN membrane, the transmission dropped sharply to 2.0 ± 0.6%, which is over 45-times lower than the corresponding result for the Durapore® membrane (93 ± 5%). The low amount of 0.18 μm

sized nanoparticles in the filtrate would suggest that a dense cake layer formed on the MSN membrane surface, rapidly occluding a portion of the slit; this observation is in in good agreement with the TMP results in Figure 3A. The experimental results for the Durapore® membrane are in good agreement with those from a previous study of nanoparticle transmission through conventional 0.22 μm membranes (Pazouki et al. 2019). While a small amount of 0.51 μm nanoparticles were seen in the filtrates from both MSN and Durapore® membranes, this was likely due to a small amount of polydispersity in the nanoparticle size (see Figure S6). A comparison of the TMP profiles for the two membranes (with two sizes of nanoparticles) is shown in Figure 3C. For the largest 0.84 μm nanoparticles, both membranes foul at a similar rate however the MSN membranes maintained a lower TMP (Figure 3C).

Finally, we evaluated the performance of the two MSN membranes with the narrower slit widths (i.e., 0.2 and 0.5 μm) to be used as sterile filters by performing a challenge test with *B. diminuta* solution (ASTM 2015). As shown in Figure 4A, there was no detectable amount of *B. diminuta* in the filtrate samples from 0.2 μm MSN membranes. To the best of our knowledge, this result represents the first demonstration of sterile filtration using slit-shaped pores. In order to confirm the accuracy of our methods, we also evaluated the performance of a conventional 0.22 μm membrane (the same Durapore® membrane) in the same bacteria challenge test and found no detectable amount of *B. diminuta* in the filtrate samples. For conventional polymer membranes, a combination of both sieving and adsorption phenomena is most often used to explain the bacterial removal mechanism (Mittelman et al. 1998). Given the very high porosity and ultrathin nature of 0.2 μm MSN membranes, however, it is most likely that adsorption effects are negligible and that the bacterial removal capability occurs exclusively via sieving by the uniform slit pores. This hypothesis is supported by the filtration test results obtained with the 0.5 μm MSN membrane which allowed the permeation of high concentrations of *B. diminuta* into the corresponding filtrate samples. Given the proper operating conditions (e.g. low applied pressure) it is likely that an intermediate slit width dimension (i.e. between 0.2 and 0.5 microns) could be used and still achieve sterile filtration performance (i.e. no detectable amount of *B. diminuta* in the filtrate). As shown in Figures 4B through 4D, the TMP profiles for the *B. diminuta* challenge test were quite consistent across the triplicate tests that were done for each membrane (similar to results in Figure 3). Our future work will further pursue the potential utility of MSN membranes' sterile filtration capability (as seen in Figure 4) for improving the post-filtration yield of large biological therapeutics in a cGMP manufacturing process.

Materials and Methods

The MSN membranes were fabricated as depicted in Figure 1A with some variations depending on the slit pore dimensions. The pores were initially patterned on the frontside of a silicon wafer, within a low-pressure chemical vapor-deposited silicon nitride layer on 150 mm diameter, 310 μm thick, double-side polished silicon wafers (WaferPro Inc). For the 0.2×10 μm slit features, deep UV (248 nm wavelength) photolithography (ASML PAS5500/300C DUV 4X Reduction Stepper) was used to pattern the slits into 500 nm thick UV™ 210 DUV positive tone photoresist (Microchemicals GmbH) and an underlying 60 nm thick Brewer Science® DUV-42P anti-reflective coating (ARC; Brewer Science Inc). The

wafers were then developed with 726 MiF (Microchemicals GmbH) and the ARC was removed via etching (27 Pa, 50 W, 20 sccm O_2, 20 sccm Ar, 75 s) using a Trion MiniLock Etcher (Trion Technology Inc). For the 0.5×50 μm and 1.0×50 μm slit features, conventional (365 nm wavelength) photolithography was used (ASML PAS5500/205 5X-Reduction Stepper) to pattern 1.2 μm thick AZ® MiR 701 positive tone photoresist (Microchemicals GmbH) and the patterned photoresist was developed in CD-26 (Microchemicals GmbH). Reactive ion etching (43 Pa, 150 W, 150 sccm He, 150 sccm SF_6, 110-220 s) for slit feature transfer was performed using a LAM 490 Etcher (LAM Systems Inc). A select number of experiments were done with nanoporous silicon nitride (NPN) membranes that were 100 nm thick with generally cylindrical pores of average 60 nm diameter; full details regarding the production of NPN membranes are available in our previous work (DesOrmeaux et al. 2014).

Following fabrication of frontside pores, the wafers' backside was processed for bulk through-wafer etching as previously described (DesOrmeaux et al. 2014) to yield approximately 400 MSN membrane chips per wafer. Resultant 0.2 μm MSN and NPN membrane chips had four 0.3×3 mm porous suspended membranes (200 nm and 100 nm thick, respectively). Resultant 0.5 and 1.0 μm MSN membrane chips had three 0.7×3 mm porous suspended membranes (400 nm thick). Scanning electron microscopy (Auriga field emission SEM, Carl Zeiss Vision Inc) at 10-20 kV acceleration voltage was used routinely to verify the pore properties. NIH Image J software was used to calculate the pore size properties and porosity from the electron micrographs.

Gas permeance and maximum differential pressure tolerance of the MSN and NPN membranes were measured by integrating them into a custom-built testing apparatus (see Figures S1 and S2). Water permeance was also measured by integrating the membranes into a different custom-built membrane holder and testing apparatus (see Figures S3 and S4).

The nanoparticle transmission tests and sterile filtration tests for the MSN membranes and Durapore® 0.22 μm PVDF membrane (MilliporeSigma) were conducted using a dedicated test apparatus containing parts that could be autoclaved before each experiment (see Figure S5). Stock solutions of fluorescent polystyrene nanoparticles with nominal diameters of 0.06, 0.18, 0.51, and 0.84 μm (Spherotech) were diluted to a concentration of 0.003% (w/v) in a 0.1 M carbonate buffer solution (Alfa Aesar), pH 9.4 with 0.01% (v/v) Tween-20. The buffer was prepared with ultra-pure water (MilliporeSigma) and pre-filtered through a 0.2 μm syringe filter. Each nanoparticle solution was placed in an ultrasonic bath for 15 minutes immediately before it was used in a filtration test. As shown in Figure S6, the sizes of nanoparticles in the prepared solutions as determined using dynamic light scattering were in good agreement with the values reported by the manufacturer. The test apparatus and membrane were first wetted and checked for leaks by passing Milli-Q water at various flow rates. Then, a disposable syringe containing the sonicated nanoparticle solution was connected to the system and passed through the membrane at a constant flux (0.8 mL cm^{-2} min^{-1}) with the filtrate collected as five to six 100 μl samples in a standard black 96-well microplate. The percent transmission of nanoparticles was determined from fluorescence intensity measurements of the filtrate and feed samples obtained via a Spark 10M microplate reader (Tecan).

The sterile filtration challenge with *B. diminuta* was performed similar to that described in ASTM F838 (2015). The test apparatus and membrane were first wetted with saline lactose broth (see Supplementary Material) and an aliquot of the filtrate from the initial wetting broth was collected and plate-cultured to confirm sterility of the test system. The syringe containing 5 mL of *B. diminuta* in saline lactose broth (see Supplementary Material) was connected to the test apparatus and then passed through the membrane at a constant flux (2 mL cm^{-2} min^{-1}) with the filtrate collected in a sterile vessel until a total of 6 mL cm^{-2} was passed through the membrane. The concentrations of *B. diminuta* in the filtrate sample and a post-filtration feed sample from the syringe were determined via triplicate analysis of the colony counts from a direct spread plate assay (incubation at 30°C for 2 days) on tryptic soy agar. Any plates that showed no colonies after 2 days were incubated for another 5 days and then checked again to confirm that no *B. diminuta* were present in the corresponding sample.

Supplementary Material

Refer to Web version on PubMed Central for supplementary material.

Acknowledgements

This work was principally funded by the National Institute of Health under Grant No. 1R43-GM128475-01. This work was performed in part at the Cornell NanoScale Science & Technology Facility (CNF), a member of the National Nanotechnology Coordinated Infrastructure (NNCI), which is supported by the National Science Foundation (Grant NNCI-1542081). Additional funding was received from the Alliance for Biotherapeutics Manufacturing Innovation project, that was supported by the Ontario Research Fund-Research Excellence program, and BioCanRx in the form of a Summer Studentship Award (to MC). SiMPore Inc., a private company, participated in this work and is commercializing the membrane material developed and used in the study.

References

ASTM (2015). F838-15a83: Standard test method for determining bacterial retention of membrane filters utilized for liquid filtration. West Conshohocken, PA: American Society for Testing and Materials.

Ausubel LJ, Hall C, Sharma A, Shakeley R, Lopez P, Quezada V, Couture S, Laderman K, McMahon R, Huang P, Hus D & Couture L (2012). Production of CGMP-grade Lentiviral vectors. BioProcess International 10(2): 32–43. [PubMed: 22707919]

Bandeira V, Peixoto C, Rodrigues AF, Cruz PE, Alves PM, Coroadinha AS & Carrondo MJ (2012). Downstream processing of lentiviral vectors: releasing bottlenecks. Human Gene Therapy, Part B: Methods, 23(4), 255–263. [PubMed: 22934827]

Bowen WR & Jenner F (1995). Theoretical descriptions of membrane filtration of colloids and fine particles: An assessment and review. Advances in Colloid and Interface Science 56, 141–200.

Bromley AJ, Holdich RG, & Cumming IW (2002). Particulate fouling of surface microfilters with slotted and circular pore geometry. Journal of Membrane Science, 196(1), 27–37.

Chandler M, & Zydney A (2006). Effects of membrane pore geometry on fouling behavior during yeast cell microfiltration. Journal of Membrane Science, 285(1), 334–342.

DesOrmeaux JPS, Winans JD, Wayson SE, Gaborski TR, Khire TS, Striemer CC, & McGrath JL (2014). Nanoporous silicon nitride membranes fabricated from porous nanocrystalline silicon templates. Nanoscale, 6(18), 10798–10805. [PubMed: 25105590]

FDA (2004). Guideline on sterile drug products produced by aseptic processing. Rockville, MD: Center for Drug Evaluation and Research, Food and Drug Administration.

Fissell WH, Dubnisheva A, Eldridge AN, Fleischman AJ, Zydney AL, & Roy S (2009). High-performance silicon nanopore hemofiltration membranes. Journal of Membrane Science, 326(1), 58–63. [PubMed: 20054402]

Gillmer SR, Fang DZ, Wayson SE, Winans JD, Abdolrahim N, DesOrmeaux JPS Getpreecharsawas J, Ellis JD, Fauchet PM & McGrath JL (2017). Predicting the failure of ultrathin porous membranes in bulge tests. Thin Solid Films, 631, 152–160.

Harp G, Cho SJ, Lester E, Rose D, Sabanyagam C, & Ross SF (2015). Microscopic Characterization of Brevundimonas diminuta in the Hydrated State. PDA Journal of Pharmaceutical Science and Technology, 69(3), 355–365. [PubMed: 26048743]

Kanani DM, Fissell WH, Roy S, Dubnisheva A, Fleischman A, & Zydney AL (2010). Permeability–selectivity analysis for ultrafiltration: Effect of pore geometry. Journal of Membrane Science, 349(1), 405–410. [PubMed: 20161691]

Kon TC, Onu A, Berbecila L, Lupulescu E, Ghiorgisor A, Kersten GF, Cui Y-Q, Amorij J-P & Van der Pol L (2016). Influenza vaccine manufacturing: effect of inactivation, splitting and site of manufacturing. Comparison of influenza vaccine production processes. PLoS One, 11(3), e0150700. [PubMed: 26959983]

Lamparski HG, Metha-Damani A, Yao JY, Patel S, Hsu DH, Ruegg C, & Le Pecq JB (2002). Production and characterization of clinical grade exosomes derived from dendritic cells. Journal of Immunological Methods, 270(2), 211–226. [PubMed: 12379326]

Meltzer TH & Jornitz MW (2003). The sterilizing filter and its pore size rating. American Pharmaceutical Review, 6, 44–53.

Mittelman MW, Jornitz MW, & Meltzer TH (1998). Bacterial cell size and surface charge characteristics relevant to filter validation studies. PDA Journal ofPpharmaceutical Science and Technology, 52(1), 37–42.

Pazouki M, Wilton AN, & Latulippe DR (2019). An experimental study on sterile filtration of fluorescently labeled nanoparticles–the importance of surfactant concentration. Separation and Purification Technology, 218, 217–226.

Shoaebargh S, Gough I, Medina MF, Smith A, van der Heijden J, Lichty BD, Bell JC & Latulippe DR (2018). Sterile filtration of oncolytic viruses: An analysis of effects of membrane morphology on fouling and product recovery. Journal of Membrane Science, 548, 239–246.

Wang Y, Hammes F, Düggelin M, & Egli T (2008). Influence of size, shape, and flexibility on bacterial passage through micropore membrane filters. Environmental Science & Technology, 42(17), 6749–6754. [PubMed: 18800559]

Warkiani ME, Wicaksana F, Fane AG, & Gong HQ (2015). Investigation of membrane fouling at the microscale using isopore filters. Microfluidics and Nanofluidics, 19(2), 307–315.

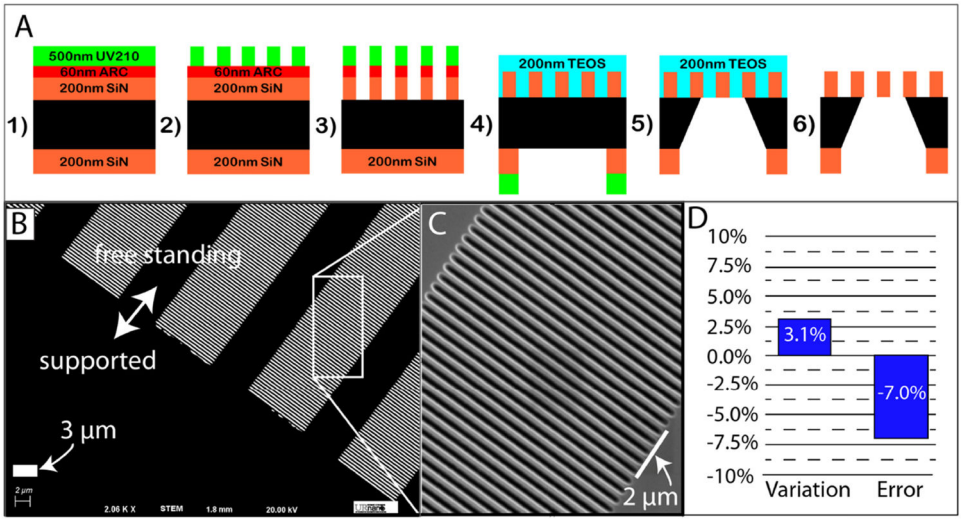

Figure 1:

Panel A): Pictographic representation (not to scale) of process workflow steps for the 0.2 µm MSN membrane: 1) deposition of SiN onto double side-polished Si wafers, followed by anti-reflective coating (ARC) and deep UV (DUV) positive photoresist onto the wafers' frontside (i.e., membrane-side); 2) photolithographic patterning by exposure of DUV photoresist; 3) transfer of slit features into the ARC (via Ar/O_2 plasma etching) and transfer into SiN (via reactive ion etching (RIE) with SF_6 and He); 4) deposition of protective SiO_2 layer (using tetra-orthoethylsilicate [TEOS]) over the transferred slit features, followed by processing on the wafers' backside to define the freestanding area and outer chip dimensions; 5) bulk through-wafer wet chemical etching; and 6) removal of the protective SiO_2 layer to form the final membrane chips with freestanding membranes.

Panel B): Scanning electron micrograph (2,060× magnification; 20 kV) of the resultant freestanding 0.2 µm MSN membranes.

Panel C): Higher magnification micrograph of a portion of the image from panel B).

Panel D): Analysis of variability between achieved and targeted slit width for 0.2 µm MSN membranes.

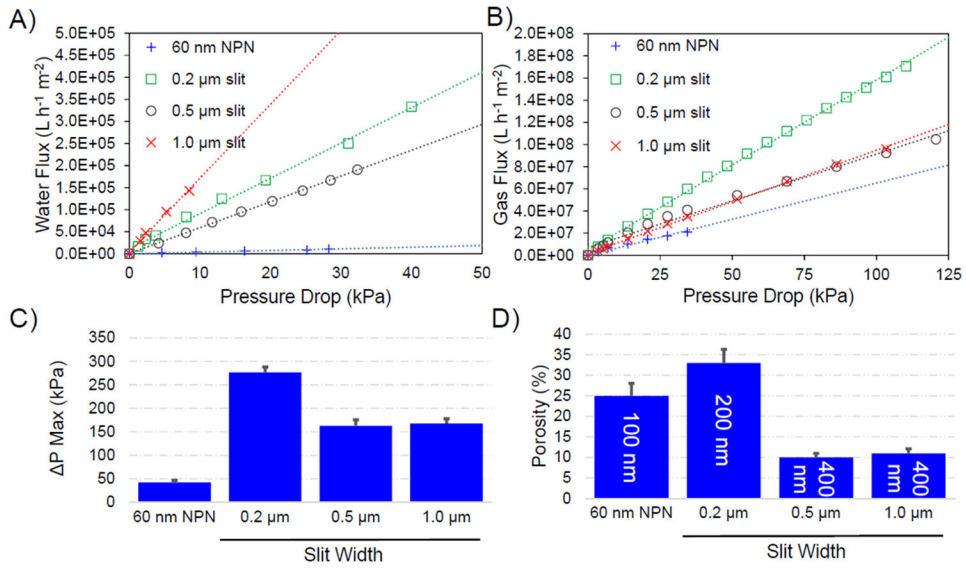

Figure 2:

Panel A): Water flux as a function of applied pressure for the three MSN membranes and one NPN membrane.

Panel B): Nitrogen gas flux as a function of applied pressure for the three MSN membranes and one NPN membrane.

For Panels A) and B), each data point represents at least triplicate observations with average error < 25% coefficient of variation (CV). The dashed lines are linear regressions of the data (Pearson's correlation coefficient $R^2 \geq 0.97$).

Panel C): Maximum differential pressure tolerance (i.e. maximum pressure reached at membrane) for the three MSN membranes and one NPN membrane; the error bars correspond to one standard deviation from the at least triplicate testing that was done for each membrane type.

Panel D): Effective porosity values for the three MSN membranes and one NPN membrane. The thickness of each membrane is given in the annotation on each vertical bar.

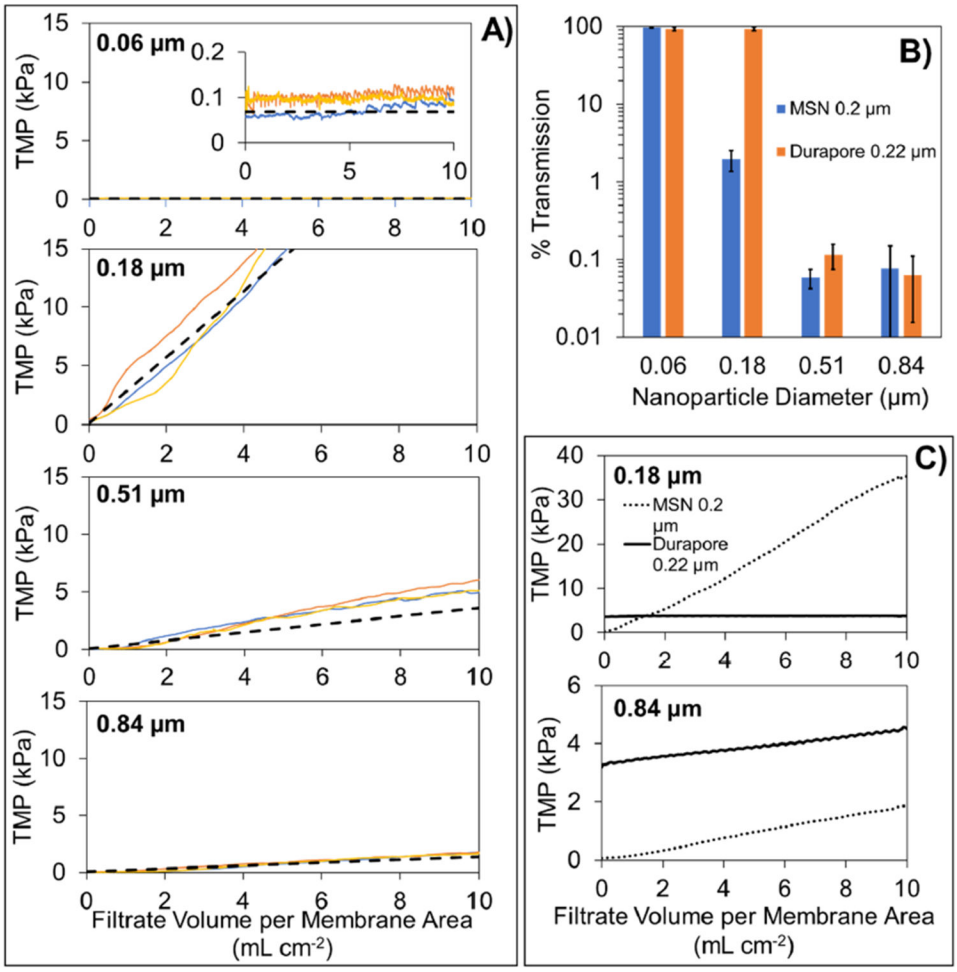

Figure 3:

Panel A): Transmembrane pressure (TMP) profiles during constant flux filtration of polystyrene nanoparticle solutions through 0.2 µm MSN membranes. The four panels correspond to the four reported sizes (0.06, 0.18, 0.51, and 0.84 µm) of polystyrene nanoparticles. The three solid colored lines within each panel correspond to the triplicate tests that were done for each size of polystyrene nanoparticle. The dashed black line within each panel corresponds to the predicted TMP profile due to formation of a cake layer on the surface of the membrane.

Panel B): Percent transmission of polystyrene nanoparticles through the 0.2 µm MSN membranes and the conventional 0.22 µm Durapore® membrane. The error bars were determined from propagation of error analysis from feed and filtrate samples collected from triplicate experiments.

Panel C): Comparison of transmembrane pressure profiles for 0.2 µm MSN membranes and conventional 0.22 µm Durapore® membranes during constant flux filtration of solutions containing 0.18 and 0.84 µm polystyrene nanoparticles. The dashed lines correspond to the average TMP profile from triplicate testing of the 0.2 µm MSN membrane (shown in panel A). The solid lines correspond to the average TMP profile from triplicate testing of the 0.22 µm Durapore® membrane.

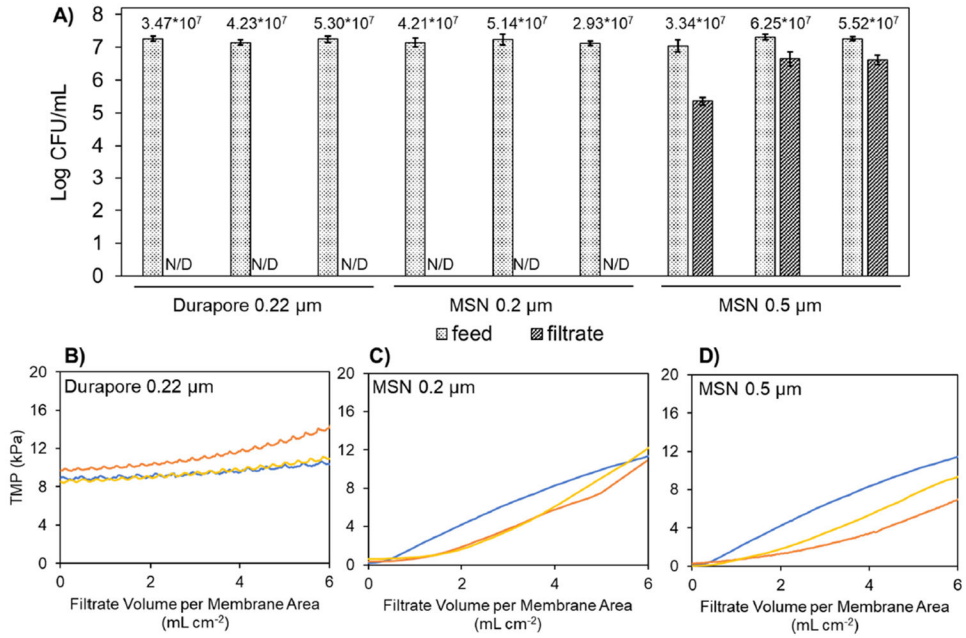

Figure 4:

Panel A): Concentration of *B. diminuta* (expressed in colony forming units (CFU) per mL) in the feed and filtrate samples from filtration tests; the error bars correspond to the standard deviation from the triplicate plate count analysis that was done on each sample. The three sets of results for each membrane type correspond to the triplicate testing as shown in panels A), B), and C). The annotations for each pair of feed and filtrate sample indicate the total challenge amount of *B. diminuta* (CFU cm^{-2}). "N/D" is used to indicate those filtrate samples for which there was no detectable amount of *B. diminuta*.

Panels B), C), and D): Transmembrane pressure (TMP) profiles during constant flux filtration of *B. diminuta* solution through a conventional 0.22 µm membrane (Durapore®), the MSN 0.2 µm membrane, and the MSN 0.5 µm membrane. The three solid colored lines within each panel correspond to the triplicate testing that was done for each membrane.